Published in final edited form as:
J Comp Neurol. 2013 October 1; 521(14): 3260–3271. doi:10.1002/cne.23345.

Quantitative Analysis of Ribbons, Vesicles, and Cisterns at the Cat Inner Hair Cell Synapse: Correlations with Spontaneous Rate

Albena Kantardzhieva, **M. Charles Liberman**, and **William F. Sewell***
Eaton-Peabody Laboratory, Department of Otology and Laryngology, Massachusetts Eye and Ear Infirmary and Harvard Medical School, Boston, Massachusetts 02114

Abstract

Cochlear hair cells form ribbon synapses with terminals of the cochlear nerve. To test the hypothesis that one function of the ribbon is to create synaptic vesicles from the cisternal structures that are abundant at the base of hair cells, we analyzed the distribution of vesicles and cisterns around ribbons from serial sections of inner hair cells in the cat, and compared data from low and high spontaneous rate (SR) synapses. Consistent with the hypothesis, we identified a "sphere of influence" of 350 nm around the ribbon, with fewer cisterns and many more synaptic vesicles. Although high- and low-SR ribbons tended to be longer and thinner than high-SR ribbons, the total volume of the two ribbon types was similar. There were almost as many vesicles docked at the active zone as attached to the ribbon. The major SR-related difference was that low-SR ribbons had more synaptic vesicles intimately associated with them. Our data suggest a trend in which low-SR synapses had more vesicles attached to the ribbon (51.3 vs. 42.8), more docked between the ribbon and the membrane (12 vs. 8.2), more docked at the active zone (56.9 vs. 44.2), and more vesicles within the "sphere of influence" (218 vs. 166). These data suggest that the structural differences between high-and low-SR synapses may be more a consequence, than a determinant, of the physiological differences.

INDEXING TERMS

synaptic ribbon; presynaptic density; active zone; vesicles; exocytosis; cochlea

Cochlear hair cells communicate via a ribbon synapse with the sensory fibers innervating them. The synaptic ribbon, a presynaptic, electron-dense structure surrounded by neurotransmitter-filled vesicles, is considered to play a role in vesicle release (Sterling and

*Correspondence to: William F. Sewell, Eaton-Peabody Laboratory, Massachusetts Eye and Ear Infirmary, 243 Charles Street, Boston, MA 02114., wfs@epl.meei.harvard.edu.

CONFLICT OF INTEREST STATEMENT
The authors report no conflict of interest.

ROLE OF AUTHORS
All authors had full access to all the data in the study and take responsibility for the integrity of the data and the accuracy of the data analysis. Study concept and design: MCL and WFS. Serial section electron microscopy: MCL. Acquisition of data: AK. Analysis and interpretation of data: AK, WFS, and MCL. Drafting and critical revision of the manuscript: AK, MCL, and WFS. Statistical analysis: AK and WFS.

Matthews, 2005; Moser et al., 2006; Glowatzki et al., 2008). It is found in hair cells and photoreceptors, cell types specialized for graded synaptic transmission. They are well adapted to release measured amounts of neurotransmitter in response to very small changes in membrane potential, to map the temporal aspects of the stimulus, and are capable of discharging at high rates for long periods of time (Logiudice et al., 2009).

Although the synaptic ribbon is the dominating anatomical characteristic of the ribbon synapse, we know little of its functional role. In mice with targeted deletion of the protein Bassoon, the synaptic ribbon detaches from the presynaptic membrane, but the changes in synaptic performance are quantitative rather than qualitative (Khimich et al., 2005; Buran et al., 2010). Although discharge rates are reduced, especially at the onset of acoustic stimuli, the postsynaptic fibers generate graded responses and are able to respond synchronously to the temporal characteristics of the stimulus.

Even less is understood of ribbon function at the cellular or molecular level. It is thought to be important for multivesicular release, either through coordinated release or through prerelease vesicular fusion (Fuchs et al., 2003; Matthews and Sterling, 2008). Others have compared it to a conveyor belt, producing a steady supply of vesicles to release sites at the presynaptic membrane (von Gersdorff et al., 1996). It may also play a role in priming vesicles for release (Zenisek, 2008; Snellman et al., 2011).

Based on our recent proteomic analysis, the synaptic-ribbon complex contains a relatively small number of major proteins, and C-terminal binding protein (CtBP) isoforms are the primary constituents (Schmitz et al., 2000; Zenisek et al., 2004; Kantardzhieva et al., 2012). CtBP's function in the ribbon is a mystery. The intimate involvement of CtBP in vesicle fission in the Golgi complex suggests a similar function in the ribbon (Weigert et al., 1999; Nardini et al., 2003; Gallop et al., 2005; Corda et al., 2006). In epithelial cells, polymorphic tubular membrane enclosures form between the Golgi complex and the basolateral membrane. They first protrude out of the Golgi along microtubules and then disengage and move toward the plasma membrane (Polishchuk et al., 2003). In the Golgi apparatus, CtBP appears at constrictions in the cisternal structure and promotes vesicle fission—the creation of new vesicles from the Golgi cisternal structures (Corda et al., 2006). When CtBP1 is inactivated (by dominant-negative mutations, siRNA, or blocking antibodies) the detachment of these protruding tubules from the Golgi complex is blocked, and in the case of dominant-negative mutations, the necks of the buds accumulate the mutant protein (Bonazzi et al., 2005; Yang et al., 2005).

We and others have hypothesized that the synaptic ribbon could be involved in the creation of new vesicles from large, endocytosed, elongated tubulo-cisterns, breaking them into new synaptic vesicles, which then remain associated with the ribbon and repopulate the vesicles at this synapse (Lenzi et al., 2002; Schwarz et al., 2011; Kantardzhieva et al., 2012). Evidence for this hypothesis is provided by the *Bassoon* knockout mouse, in which the ribbon detaches from the synapse and the endocytic membrane retrieval remains normal, but tubular and cisternal membrane structures accumulate at the synapse (Khimich et al., 2005). These displaced ribbons appear to attract and accumulate many membranous structures around them. Interestingly, similar membranous structures are also observed at the ribbon

synapses following intense stimulation (Lenzi et al., 2002; Holt et al., 2003). Schwarz et al. (2011) describe synaptic ribbons as hotspots for generation of phosphatidic acid. Phosphatidic acid is necessary for inducing membrane curvature in vesicle fission (Weigert et al., 1999; Bonazzi et al., 2005; Cazzolli et al., 2006; Corda et al., 2006; Oude Weernink et al., 2007).

Despite an abundance of immunohistochemical and ultrastructural documentation of the synaptic ribbon, there are few quantitative or objective data on the distribution of vesicles and larger membranous structures around the ribbon, especially in the mammal. However, the mammalian cochlea provides an unparalleled opportunity to correlate ribbon structure with function, because each afferent fiber makes only one synaptic contact with the hair cell, and the two types of afferent fibers that contact each inner hair cell have very different functional characteristics (Pfeiffer and Kiang, 1965; Liberman, 1982a; Merchan-Perez and Liberman, 1996). High spontaneous rate (SR) fibers, or synapses, discharge in the absence of acoustic stimulation at rates of 20 to 120 sp/sec and have very low thresholds to acoustic stimulation, as well as narrow dynamic ranges in response to changing stimulus intensity (Taberner and Liberman, 2005). Low-SR synapses have little or no spontaneous discharge and have high thresholds to acoustic stimulation and larger dynamic ranges.

In this study, we analyze the distribution of vesicles and tubulo-cisternal structures around synaptic ribbons, as reconstructed from serial sections through the inner hair cell synaptic zone, comparing data from low- and high-SR synapses. The two types of synapses are distinguished based on location around the hair cell circumference and on the mitochondrial content of their associated terminals (Liberman, 1980; Merchan-Perez and Liberman, 1996). Consistent with the idea that the ribbon converts cisterns to vesicles, we found fewer cisternal structures and more synaptic vesicles close to the ribbons. The ribbon appears to have a sphere of influence on the distribution of the vesicles and cisterns around it, which extends for ~350 nm. A comparison of low- versus high-SR synapses revealed more similarities than differences, suggesting a minimal role of the ribbon in the functional differentiation of these two types of synapses.

MATERIALS AND METHODS

Electron micrographs of complete serial sections through all the ribbon synapses from several cochlear inner hair cells in cat were generated in a prior study of the synaptic ribbon, and complete details on the material and its treatment are described there (Liberman, 1980). In brief, the cochlea from a 6-month-old cat raised in a low-noise chamber was fixed with intralabyrinthine perfusion of 2.5% glutaraldehyde/0.1 M phosphate buffer containing 0.005% Ca Cl_2, pH 7.2, at 4°C. The tissue was also postfixed for 2 hours in 1.5% osmium tetraoxide/0.1 M phosphate buffer; dehydrated, and embedded in Epon. The cochlear spiral was cut into 1-mm pieces, and the pieces containing fibers of characteristic frequency between 2.6 and 2.2 kHz were used for electron microscopy. Two adjacent hair cells were chosen for the study. Before histological processing, responses from several hundred cochlear nerve fibers were collected in each animal; thus the normality of the cochlear responses in these cases has been amply documented (Liberman, 1980).

Each synaptic ribbon spanned three to seven sections (70-nm thickness, cut parallel to the reticular lamina). Electron micrographs (10,000×) were scanned and digitized to create 16-bit images, on which digital measurements were made by using Adobe Photoshop CS5, and CS4 extended version (Adobe Systems, San Jose, CA). Afferent synapses were categorized as high-or low-SR based on location around the inner hair cell circumference (modiolar for low-SR and pillar for high-SR) and mitochondrial count in the postsynaptic nerve terminals (high in high-SR and low in low-SR). The mito-chondrial content was established by counting mito-chondrial profiles through the unmyelinated segment of the afferent fiber, and is expressed as profiles/cross section (Liberman, 1980, b; Liberman et al., 1990) (Table 1). We analyzed six ribbon synapses contacting fibers with the highest mitochondrial count (high-SR synapses) and six contacting fibers with the lowest mitochondrial count (low-SR synapses). To quantify the size and position of vesicles and cisternal structures, each membrane-enclosed structure in each micrograph through the synaptic ribbon was outlined, and measurements of area, perimeter, and circularity were recorded. Next, we measured the distance between each structure and three reference points: A) the point on the ribbon closest to it; B) the point on the ribbon closest to the inner hair cell [IHC] membrane); and C) the point on the IHC membrane closest to the vesicle/cistern in question (Fig. 1). Because the program could not estimate the center of gravity of these outlines, we used the edge closest to the reference. Since average vesicle diameter is 41.6 nm (Fig. 1), we added 21 nm to approximate the distance to the center of the vesicle.

We analyzed vesicles and cisterns within ~1 μm from the ribbon base at the IHC membrane, which corresponds to roughly half the average distance between adjacent ribbons in the mammalian cochlea (Meyer et al., 2009). This was also the maximal distance with relatively complete coverage of the presynaptic area in all directions away from the ribbon base. For each section, the analysis area was divided into concentric rings, each 44 nm thick. Thus, the area with radius of 924 nm was covered by 21 rings. The total area of the hair cell visible in each micrograph was calculated to estimate the percentage of hair cell cytoplasm in the synaptic region that is occupied by vesicles and cisterns (Table 1). The presynaptic active zone of the hair cell was defined as the electron-dense, thickened area symmetrically opposed by an electron-dense region on the postsynaptic afferent neuron. We also separately quantified the pre- and postsynaptic densities.

RESULTS

Defining vesicles and cisterns

Synaptic ribbons innervating high- versus low-SR fibers were identified based on their location and the mitochondrial content of their adjacent afferent nerve terminals (see Materials and Methods). We measured the perimeters and cross-sectional areas of the ribbons, and then calculated the surface area and volume of the synaptic ribbons from all the reconstructed synapses (Table 1). The average surface area of the high-SR ribbons was 14% less than that for low-SR ribbons. However, because high-SR ribbons tended to be shorter (245 vs. 338 nm) and rounder than low-SR ribbons, there was only a small (4%) difference in volume (Table 1).

The cytoplasm surrounding the synaptic ribbon is densely packed with membranous structures: some are small and round, while others are large and complex in shape. We classified these structures as synaptic vesicles or cisterns by defining the small, round structures immediately adjacent, and often attached, to the ribbon as synaptic vesicles (Paillart et al., 2003; Spassova et al., 2004). A Gaussian curve fit to measurements of 753 such vesicles from several synapses indicated a median cross-sectional area of 1,305 nm^2, (σ =280) or a diameter of 40.7 nm. A histogram of the cross-sectional areas of all membranous structures in the synaptic region (Fig. 2A) indicated that a large percentage were the size of synaptic vesicles. However, the skew toward higher areas suggested several populations with different sizes. The distribution was well fit as the sum of four Gaussian distributions. The largest population, comprising 62% of all membrane-enclosed structures, was virtually indistinguishable in size (1,359 nm^2 [σ =250 nm^2] or 41.6 nm in diameter) from the ribbon-adjacent synaptic vesicles (1,305 nm^2 [σ =280 nm^2]. A small group (4%) of slightly larger vesicles (1,979 nm^2 [σ =140 nm^2], diameter =50.2 nm) constituted a narrow peak. A third population, constituting 21%, had a broad range of sizes centered at 2,226 nm^2 [σ=800 nm^2], diameter =53.2 nm). A fourth population of 10.4% had a very broad range of areas with a median of 5,050 nm^2 [σ =2,000 nm^2]. The remaining 3% were large structures with areas greater than 10,000 nm^2 (Fig. 2B).

For subsequent analysis, synaptic vesicles were defined as any membranous structure within 3 standard deviations of the mean area of ribbon-attached vesicles, thus defining a maximum vesicle area of 2,147 nm^2 (diameter =52.3 nm). With this criterion, approximately 76% of the membranous structures were classified as vesicles, although they represented only 43.5% of the total area of the membranous structures. The percentage of the presynaptic space occupied by vesicles was similar for high- versus low-SR synapses (Table 1).

Because the analysis indicated that two other populations might overlap in size with the synaptic vesicles, we examined the images for evidence of multiple populations based on criteria other than area. The small (4%) group, with mean area of 1,979 nm^2, may reflect overlap between two vesicles within the same section, appearing as a single, slightly larger structure. However, there was no obvious way, other than size, to distinguish among vesicles from these three putative groups; we could distinguish no differences based on circularity or any other morphological criterion. However, an analysis of distribution as a function of distance from the ribbon suggests that the group with mean area of 2,226 nm^2 distributes more like cisterns than vesicles (see below).

Spatial distributions of vesicles versus cisterns

The spatial distribution of vesicles and cisterns near the ribbon is illustrated in Figure 3, where vesicles or cisterns from three adjacent serial sections are superimposed and color-coded. Cisternal structures appear to be reduced in density near the synaptic ribbon, whereas vesicles are denser near the ribbon. To quantify the density of vesicles and cisterns as a function of distance from the ribbon, we divided the area around the ribbon into concentric rings. The midpoint of each ring was positioned at the ribbon center, assuming a circular ribbon with an average diameter calculated from cross-sectional area for the low- or high-SR synapses.

Vesicle density was highest (~6,000 vesicles/μm^3) immediately adjacent to the ribbon surface and decreased over the next few hundred nanometers. Beyond 350 nm, the density distribution reached an asymptote at roughly 600 vesicles/μm^3 (Fig. 4A). Low-SR synapses had more vesicles at distances between 124 and 308 nm from the ribbon surface than did high-SR synapses (P =0.007 by Student's t-test). Each synaptic ribbon had, on average, 47.1 (± 4.4 SE) vesicles within 30 nm of its surface. (We did not account for vesicles in the sections at either end of each series, where the ribbon was not present.) For high-SR synapses, the mean vesicle count within 30 nm of the ribbon's surface was 42.8 (± 3.3) versus 51.3 (±8.3) for low-SR versus high-SR synapses, a difference of 17%. This was similar to the difference in surface area of the ribbon for low- versus high-SR synapses, and consistent with our observation that the density of attached vesicles on the ribbon surface (~360 vesicles/μm^2) is similar for low- versus high-SR synapses (Table 1).

For both high- and low-SR synapses, there were fewer cisternal structures near the ribbon, and the number increased with increasing distance from the ribbon until an asymptote was reached at approximately 350 nm (Fig. 4B). Within 1 μm of the ribbon surface, the average low-SR synapse had 96 cisterns compared with 88 for the high-SR synapse, and the total area occupied by the cisterns for low-SR synapses was larger than for high-SR synapses (see also Table 1). Due to the complicated shapes of the cisterns, and their span over several concentric rings, we did not attempt to estimate their density as a function of distance from the ribbon.

Synaptic release sites are assumed to be beneath the synaptic ribbon, although release away from the ribbon has also been suggested (Zenisek, 2008; Zenisek et al., 2003). The synaptic ribbon sits near the presynaptic density, where the voltage-activated calcium channels are clustered (Roberts et al., 1990; Zenisek et al., 2003; Zenisek, 2008; Frank et al., 2010). We have demarcated the active zone as the electron-dense area symmetrically opposed by specialized membrane postsynaptically. The mean width of the active zone for sections containing ribbon was 727 (±16) nm and was not significantly different for low- versus high-SR synapses (Table 1). These values are intermediate between those reported for turtle (~560 nm; Schnee et al., 2005) and mouse (~850 nm; Meyer et al., 2009). The total surface area of the active zone was 343,778 (±33,879) nm^2, and was similar for high-and low-SR synapses (Table 1). The ribbon was positioned centrally (Figs. 1, 3); thus the active zone spanned, on average, 350–380 nm on each side of the ribbon.

To assess whether vesicles tended to cluster at the presynaptic membrane near the ribbon, we analyzed the density of vesicles docked at the presynaptic membrane. We considered vesicles within 20 nm of the pre-synaptic membrane to be docked, consistent with Graydon et al. (2011), who based this distance on the approximate length of the SNARE proteins tethering vesicles (Hohl et al., 1998). Docked vesicle density at the active zone was higher for low-SR synapses (158 ± 18.2 SE vesicles/μm^2) than for high-SR synapses (145 ± 20.9 SE vesicles/μm^2). The density varied with distance from the base of the ribbon (Fig. 5A), being higher nearest the base of the ribbon. The vesicle density at the active zone was significantly higher for the low-SR synapses at distances of 88–176 nm from the ribbon base (P =0.004 by Student's t-test). These data are a subset of the data presented in Figure 4A, and show a similar distribution pattern. Peak values were seen within 100 nm of the ribbon

base (Fig. 5A), as also observed in vestibular hair cell and bipolar cell ribbon synapses (Lenzi et al., 1999; von Gersdorff et al., 1996).

For cisterns, the distribution was opposite that for the vesicles. There were few membrane-adjacent cisterns at the base of the ribbon, but their number increased gradually, to a plateau after 350 nm (Fig. 5B). This pattern is similar to the general cistern distribution around the ribbon presented in Figure 3.

The size distribution of membranous structures suggested a population (solid gray line in Fig. 2) larger than synaptic vesicles, but smaller than cisterns. To analyze the distribution of this population of membranous structures, we included all structures larger than vesicles (2,148 nm^2 and smaller than 4,200 nm^2 (Fig. 2). The distribution of these structures was compared with that of vesicles (not shown) and with that of the larger cisternal structures (size over 4,200 nm^2). These intermediate-sized membranous structures behaved like the rest of the cisterns, showing an increased distribution with distance from the ribbon's surface (Fig. 6).

Vesicle pools

We quantified the number of vesicles in each of four pools defined based on anatomical location: 1) a *ribbon-attached pool*, i.e., within 30 nm of the ribbon surface; 2) an *immediately releasable pool*, i.e., those ribbon-attached vesicles immediately beneath the ribbon at the active zone; 3) a *docked pool*, i.e., within 20 nm of the presynaptic density but not within the immediately releasable pool, and 4) a *proximal free pool*, i.e., not attached to the ribbon or docked at the membrane, but within its sphere of influence of 350 nm (Fig. 7) (Lenzi et al., 1999; Schnee et al., 2005; Graydon et al., 2011). In the present study (Table 1), the average high-SR synapse had 42.8 ribbon-attached vesicles, 8.2 of which were within the immediately releasable pool, 44.2 docked vesicles, and 78.5 vesicles in the proximal free pool, for a total of 165.5 vesicles within a 350-nm radius of the ribbon surface. The average low-SR synapse had 51.3 ribbon-attached vesicles, with 12 in the immediately releasable pool, 56.9 active-zone-docked vesicles, and 109.7 in the proximal free pool, for a total of 217.9 vesicles. Thus, the high-SR synapses appear to have a smaller vesicle reserve available for release, which could be viewed as a result of their high firing rates.

DISCUSSION

We have identified a "sphere of influence" around the synaptic ribbon of 350 nm, where the number and size of cisternal structures is decreased and the density of synaptic vesicles is increased. This radius coincides with the size of the active zone, which extends roughly 350–380 nm on each side of the ribbon. This is also the region with the greatest differences between high-and low-SR synapses, suggesting that the region is functionally dynamic.

Because high- and low-SR synapses coexist on the same hair cell, yet differ so markedly in discharge rate and threshold to acoustic stimulation, we expected that a quantitative comparison of the ribbon and its associated vesicle pools would show differences that could provide insight into the role of the ribbon. Perhaps the most remarkable feature of our analysis is the similarity between the two types of synapses. Although high- and low-SR

ribbons show differences in their structure (low-SR ribbons tend to be longer and thinner), the total volume of the two ribbon types is similar. As previously reported, low-SR ribbons have more vesicles on their ribbon surfaces, but we found this is only in proportion to their increased surface area (Merchan-Perez and Liberman, 1996). In fact, low- and high-SR ribbons are coated with vesicles at similar surface densities.

A major difference observed was that low-SR ribbons had more synaptic vesicles intimately associated with them compared with high-SR synapses. Low-SR synapses had more vesicles attached to the synaptic ribbon (51.3 vs. 42.8), more vesicles docked between the ribbon and the presynaptic membrane (12 vs. 8.2), more vesicles docked at the presynaptic membrane (56.9 vs. 44.2), and more in the proximal free pool (not ribbon-attached or docked) within the 350-nm sphere of influence (109.7 vs. 78.5; P =0.015). These data suggest that the structural differences between high- and low-SR synapses may be more a consequence, than a determinant, of their physiological differences. The observed differences might indicate that the higher rate of vesicle release at high SR-synapses taxes the ability of the synapse to build up reserves of vesicles in the regions near the ribbons. If one function of the ribbon is to create new vesicles from cisterns, then, despite the smaller pool of vesicles, the high-SR ribbons may be more active in creating vesicles to compensate for this putative vesicle depletion.

Our observations also highlight an unappreciated feature of the ribbon synapse, i.e., that there are almost as many vesicles docked at the active zone as are attached to the synaptic ribbon. Whereas the density of docked vesicles is only one-third that of ribbon-attached vesicles, the area of the active zone is nearly three times the surface area of the ribbon. Thus, the size of the two pools is similar. Perhaps this is part of the reason why the *Bassoon* knockout mice, in which most synapses lack ribbons, have surprisingly little synaptic dysfunction (Khimich et al., 2005; Buran et al., 2010). This finding also has implications for the identity of the “readily releasable pool,” as estimated from capacitance measurements (Spassova et al., 2004; Schnee et al., 2005; Graydon et al., 2011). Although the pool size estimated from the physiology is similar to the number of vesicles tethered to the ribbon, the present results show that it is also similar to the number of vesicles docked at the presynaptic membrane. Interestingly, the density of fusion-competent vesicles at the active zone in photoreceptors (150/μm^2; Zampighi et al., 2011) is nearly identical to the density (151/μm^2) we calculated for docked vesicles at the hair cell’s active zone.

Several other detailed quantitative analyses of vesicles at ribbon synapses have been published, one for frog vestibular hair cells (Lenzi et al., 1999), one for frog amphibian papilla (an auditory organ; Graydon et al., 2011), and one in the turtle basilar papilla (also an auditory organ; Schnee et al., 2005), as well as a limited analysis for the mouse (Khimich et al., 2005). Our data from the cat show a number of similarities.

First, the density of vesicles on the surface of the ribbon is similar for all ribbons studied: combining low-and high-SR synapses yields an average of 362 vesicles/μm^2 of ribbon surface, similar to that in the bullfrog saccule (413 vesicles/μm^2, calculated from Lenzi et al., 1999); the turtle basilar papilla (468 vesicles/μm^2, calculated from Schnee et al., 2005), and the frog amphibian papilla (566 vesicles/μm^2, calculated from Graydon et al., 2011),

suggesting that vesicle packing on the surface of the ribbon reflects some fundamental property of the ribbon rather than functional properties of the synapse, although the ribbon-associated pool can be reduced with intense stimulation (Lenzi et al., 2002).

Second, our assessment of the number of vesicles docked between the ribbon and the presynaptic membrane (using a similar criterion for the immediately releasable pool as that reported by Graydon et al. [2011], i.e., vesicles docked within 20 nm of the pre-synaptic membrane and within 30 nm of the ribbon) was similar to those made in several other hair cell systems. We observed 10.1 vesicles in this pool, comparable to Graydon et al. (2011), who observed 12.6 vesicles in the amphibian papilla, and Khimich et al. (2005), who observed 16–30 in the mouse. Estimates from the turtle organ of hearing are higher (28–32; Schnee et al., 2005). Our observation of 10.1 vesicles in this pool is also similar to an estimate of 12 vesicles inferred from afferent fiber excitatory postsynaptic currents (EPSCs) from the rat cochlea (Goutman and Glowatzki, 2007), but lower than estimates of 27 in the gerbil cochlea (Johnson et al., 2009), 53–64 in the mouse cochlea (Khimich et al., 2005), and 41 in the chick basilar papilla (Spassova et al., 2004).

A comparison of our and others' anatomical data with published physiological measurements suggests that vesicles may be recruited or generated at the synapse. The density of vesicles that we measured in the cytoplasm ~1 mm away from the ribbon (600 vesicles/μm^3), was very close to that reported in the turtle (535 vesicles/μm^3; Schnee et al., 2005) and the frog (851 vesicles/μm^3; Graydon et al., 2011). However, these numbers of vesicles are insufficient to maintain the high rates of vesicle release as estimated from changes in membrane capacitance (Graydon et al., 2011). Goutman and Glowatzki (2007) describe, based on afferent fiber whole-cell recording in the mammal, an adapting component of the synaptic response comprising release of 216 vesicles. This corresponds remarkably well with the total numbers of vesicles found within the 350-nm sphere of influence, including docked and ribbon attached, which were, respectively, 217.9 and 165.5 vesicles in low- and high-SR synapses. This raises the possibility that all of the vesicles in the sphere of influence are available for rapid release and that vesicle release following adaptation may be limited by rates of generation of recruitment of vesicles within that region.

The curve fit of membrane-enclosed structures at the synapse (Fig. 2) indicated an intermediate-sized population of structures with a median diameter of 53.2 nm. If these structures are competent for fusion and released, they would likely result in the release of greater quantities of neurotransmitter than the smaller, more stereotyped synaptic vesicles. Glowatzki and coworkers (Glowatzki and Fuchs, 2002, Grant et al., 2010) observed, at the inner hair cell synapse, a distribution of EPSC amplitudes with a long tail due to the presence of many larger events; they interpret the long tail as being due to fusion or synchronized multivesicular release of vesicles. Our observation of a population of larger membrane-enclosed structures suggests an alternate (albeit untested) possibility: instead of many vesicles, perhaps one or a few of these larger membrane-enclosed structures are released to generate the larger synaptic events.

Endocytosis occurs in ribbon synapses following intense stimulation, such that the membrane added to the presynaptic cell by vesicle fusion is recycled and broken down to form new synaptic vesicles (Lenzi et al., 2002; Holt et al., 2003, 2004; Matthews and Sterling, 2008). The idea that the ribbon creates vesicles from larger cisternal structures is supported by electron tomography analysis of ribbon synapses in frog hair cells, where synaptic inhibition increased vesicle counts on ribbons, and in nearby cytoplasm, whereas synaptic excitation depleted over 70% of the vesicles near the synapse and increased intracellular cisterns and membrane invaginations accounting for most of the vesicular membrane loss (Lenzi et al., 2002). Ribbon-attached vesicles were depleted mostly in the part facing the presynaptic membrane, creating a gradient of vesicles around the ribbon surface. The authors conclude that formation of new synaptic vesicles from the observed cisterns and membrane invaginations is the rate-limiting step in vesicle recycling (Lenzi et al., 2002). In fact, Cho et al. (2011) have demonstrated fast endocytosis of membrane during brief depolarizations with a limited temporal capacity for vesicle replenishment.

The synaptic ribbon contains large quantities of CtBP proteins (Schmitz et al., 2000; Zenisek et al., 2004; Kantardzhieva et al., 2012). They may have a membrane-partitioning function similar to that seen in the Golgi apparatus, i.e., forming vesicles from cisternal structures (Weigert et al., 1999; Nardini et al., 2003; Gallop et al., 2005; Corda et al., 2006). Ribeye is composed of a unique amino-terminal A domain, which contributes a structural stability to the synaptic ribbon, and a C-terminal B domain, which is very similar to that of CtBP2 (Schmitz et al., 2000; Magupalli et al., 2008; Schmitz, 2009). Ribeye's B domain has lysophosphatidic acid acyltransferase activity, and transfers palmitoyl-CoA to lysophosphatidic acid to generate phosphatidic acid, thus enriching it in the vicinity of synaptic ribbons (Schwarz et al., 2011). Phosphatidic acid is a cone-shaped lipid, which induces the negative membrane curvature that is required for membrane fusion and fission (Weigert et al., 1999; Bonazzi et al., 2005; Cazzolli et al., 2006; Corda et al., 2006; Oude Weernink et al., 2007). Importantly, cone-shaped lipids such as phosphatidic acid are required for the formation of a stalk-like hemifusion intermediate (Chernomordik and Kozlov, 2005; Chernomordik et al., 2006). Ribbon-generated phosphatidic acid may provide the negative membrane curvature needed for vesicle fission, similarly to CtBP1 in the Golgi (Bonazzi et al., 2005).

Mammalian ribbon synapses can release vesicles over long periods (tens of minutes), at high rates (hundreds per second), whereas conventional synapses can sustain such release for only 100 ms at best (Parsons et al., 1994; Moser and Beutner, 2000; Goutman and Glowatzki, 2007). The majority of evoked vesicle release is thought to occur in close vicinity to the ribbon (Zenisek et al., 2003; Zenisek, 2008). The accessibility of large pools of vesicles available for release, apart from the ones attached to the ribbon, suggests that the ribbon is reloaded with vesicles from the proximal pool (Eisen et al., 2004; Griesinger et al., 2005). We suggest another aspect of this picture: the de novo creation of vesicles via cisternal fission by the ribbon to repopulate the pools. The fact that we rarely see large cisternal structures close to the ribbon implies either a very fast process of perhaps partial disintegration of the ribbon in the process of creating new vesicles at some distance from its surface. Although understanding this process will take considerable effort, the present analysis provides support for the hypothesis and suggests a regional influence of the ribbon

of about 350 nm, a quantitative metric that can constrain molecular explanations of the phenomenon.

Acknowledgments

We thank our colleagues Dr. Ruth Anne Eatock and Dr. Christian Brown for their critical review of the manuscript.

Grant sponsor: the National Institute on Deafness and Other Communication Disorders; Grand numbers: DC00767 and DC09651 (to W.F.S.) and DC0188 (to M.C.L.); Grant sponsor: the Hearing Health Foundation (to A.K.).

LITERATURE CITED

Bonazzi M, Spano S, Turacchio G, Cericola C, Valente C, Colanzi A, Kweon HS, Hsu VW, Polishchuck EV, Polish-chuck RS, Sallese M, Pulvirenti T, Corda D, Luini A. CtBP3/BARS drives membrane fission in dynamin-independent transport pathways. Nat Cell Biol. 2005; 7:570–580. [PubMed: 15880102]

Buran BN, Strenzke N, Neef A, Gundelfinger ED, Moser T, Liberman MC. Onset coding is degraded in auditory nerve fibers from mutant mice lacking synaptic ribbons. J Neurosci. 2010; 30:7587–7597. [PubMed: 20519533]

Cazzolli R, Shemon AN, Fang MQ, Hughes WE. Phospholipid signalling through phospholipase D and phosphatidic acid. IUBMB Life. 2006; 58:457–461. [PubMed: 16916782]

Chernomordik LV, Kozlov MM. Membrane hemifusion: crossing a chasm in two leaps. Cell. 2005; 123:375–382. [PubMed: 16269330]

Chernomordik LV, Zimmerberg J, Kozlov MM. Membranes of the world unite! J Cell Biol. 2006; 175:201–207. [PubMed: 17043140]

Cho S, Li GL, von Gersdorff H. Recovery from short-term depression and facilitation is ultrafast and Ca2+ dependent at auditory hair cell synapses. J Neurosci. 2011; 31:5682–5692. [PubMed: 21490209]

Corda D, Colanzi A, Luini A. The multiple activities of CtBP/BARS proteins: the Golgi view. Trends Cell Biol. 2006; 16:167–173. [PubMed: 16483777]

Eisen MD, Spassova M, Parsons TD. Large releasable pool of synaptic vesicles in chick cochlear hair cells. J Neurophysiol. 2004; 91:2422–2428. [PubMed: 14749306]

Frank T, Rutherford MA, Strenzke N, Neef A, Pangrsic T, Khimich D, Fejtova A, Gundelfinger ED, Liberman MC, Harke B, Bryan KE, Lee A, Egner A, Riedel D, Moser T. Bassoon and the synaptic ribbon organize Ca(2)+ channels and vesicles to add release sites and promote refilling. Neuron. 2010; 68:724–738. [PubMed: 21092861]

Fuchs PA, Glowatzki E, Moser T. The afferent synapse of cochlear hair cells. Curr Opin Neurobiol. 2003; 13:452–458. [PubMed: 12965293]

Gallop JL, Butler PJ, McMahon HT. Endophilin and CtBP/BARS are not acyl transferases in endocytosis or Golgi fission. Nature. 2005; 438:675–678. [PubMed: 16319893]

Glowatzki E, Fuchs P. Transmitter release at the hair cell ribbon synapse. Nat Neurosci. 2002; 5:147–154. [PubMed: 11802170]

Glowatzki E, Grant L, Fuchs P. Hair cell afferent synapses. Curr Opin Neurobiol. 2008; 18:389–395. [PubMed: 18824101]

Goutman JD, Glowatzki E. Time course and calcium dependence of transmitter release at a single ribbon synapse. Proc Natl Acad Sci U S A. 2007; 104:16341–16346. [PubMed: 17911259]

Grant L, Yi E, Glowatzki E. Two modes of release shape the postsynaptic response at the inner hair cell ribbon synapse. J Neurosci. 2010; 30:4210–4220. [PubMed: 20335456]

Graydon CW, Cho S, Li GL, Kachar B, von Gersdorff H. Sharp Ca(2)(+) nanodomains beneath the ribbon promote highly synchronous multivesicular release at hair cell synapses. J Neurosci. 2011; 31:16637–16650. [PubMed: 22090491]

Griesinger CB, Richards CD, Ashmore JF. Fast vesicle replenishment allows indefatigable signalling at the first auditory synapse. Nature. 2005; 435:212–215. [PubMed: 15829919]

Hohl TM, Parlati F, Wimmer C, Rothman JE, Sollner TH, Engelhardt H. Arrangement of subunits in 20 S particles consisting of NSF, SNAPs, and SNARE complexes. Mol Cell. 1998; 2:539–548. [PubMed: 9844627]

Holt M, Cooke A, Wu MM, Lagnado L. Bulk membrane retrieval in the synaptic terminal of retinal bipolar cells. J Neurosci. 2003; 23:1329–1339. [PubMed: 12598621]

Holt M, Cooke A, Neef A, Lagnado L. High mobility of vesicles supports continuous exocytosis at a ribbon synapse. Curr Biol. 2004; 14:173–183. [PubMed: 14761649]

Johnson SL, Franz C, Knipper M, Marcotti W. Functional maturation of the exocytotic machinery at gerbil hair cell ribbon synapses. J Physiol. 2009; 587:1715–1726. [PubMed: 19237422]

Kantardzhieva A, Peppi M, Lane WS, Sewell WF. Protein composition of immunoprecipitated synaptic ribbons. J Proteome Res. 2012; 11:1163–1174. [PubMed: 22103298]

Khimich D, Nouvian R, Pujol R, Tom Dieck S, Egner A, Gundelfinger ED, Moser T. Hair cell synaptic ribbons are essential for synchronous auditory signalling. Nature. 2005; 434:889–894. [PubMed: 15829963]

Lenzi D, Runyeon JW, Crum J, Ellisman MH, Roberts WM. Synaptic vesicle populations in saccular hair cells reconstructed by electron tomography. J Neurosci. 1999; 19:119–132. [PubMed: 9870944]

Lenzi D, Crum J, Ellisman MH, Roberts WM. Depolarization redistributes synaptic membrane and creates a gradient of vesicles on the synaptic body at a ribbon synapse. Neuron. 2002; 36:649–659. [PubMed: 12441054]

Liberman MC. Morphological differences among radial afferent fibers in the cat cochlea: an electron-microscopic study of serial sections. Hear Res. 1980; 3:45–63. [PubMed: 7400048]

Liberman MC. The cochlear frequency map for the cat: labeling auditory-nerve fibers of known characteristic frequency. J Acoust Soc Am. 1982a; 72:1441–1449. [PubMed: 7175031]

Liberman MC. Single-neuron labeling in the cat auditory nerve. Science. 1982b; 216:1239–1241. [PubMed: 7079757]

Liberman MC, Dodds LW, Pierce S. Afferent and efferent innervation of the cat cochlea: quantitative analysis with light and electron microscopy. J Comp Neurol. 1990; 301:443–460. [PubMed: 2262601]

Logiudice L, Sterling P, Matthews G. Vesicle recycling at ribbon synapses in the finely branched axon terminals of mouse retinal bipolar neurons. Neuroscience. 2009; 164:1546–1556. [PubMed: 19778591]

Magupalli VG, Schwarz K, Alpadi K, Natarajan S, Seigel GM, Schmitz F. Multiple RIBEYE-RIBEYE interactions create a dynamic scaffold for the formation of synaptic ribbons. J Neurosci. 2008; 28:7954–7967. [PubMed: 18685021]

Matthews G, Sterling P. Evidence that vesicles undergo compound fusion on the synaptic ribbon. J Neurosci. 2008; 28:5403–5411. [PubMed: 18495874]

Merchan-Perez A, Liberman MC. Ultrastructural differences among afferent synapses on cochlear hair cells: correlations with spontaneous discharge rate. J Comp Neurol. 1996; 371:208–221. [PubMed: 8835727]

Meyer AC, Frank T, Khimich D, Hoch G, Riedel D, Chapochnikov NM, Yarin YM, Harke B, Hell SW, Egner A, Moser T. Tuning of synapse number, structure and function in the cochlea. Nat Neurosci. 2009; 12:444–453. [PubMed: 19270686]

Moser T, Beutner D. Kinetics of exocytosis and endocytosis at the cochlear inner hair cell afferent synapse of the mouse. Proc Natl Acad Sci U S A. 2000; 97:883–888. [PubMed: 10639174]

Moser T, Brandt A, Lysakowski A. Hair cell ribbon synapses. Cell Tissue Res. 2006; 326:347–359. [PubMed: 16944206]

Nardini M, Spano S, Cericola C, Pesce A, Massaro A, Millo E, Luini A, Corda D, Bolognesi M. CtBP/BARS: a dual-function protein involved in transcription co-repression and Golgi membrane fission. EMBO J. 2003; 22:3122–3130. [PubMed: 12805226]

Oude Weernink PA, Lopez de Jesus M, Schmidt M. Phospholipase D signaling: orchestration by PIP2 and small GTPases. Naunyn Schmiedebergs Arch Pharmacol. 2007; 374:399–411. [PubMed: 17245604]

Paillart C, Li J, Matthews G, Sterling P. Endocytosis and vesicle recycling at a ribbon synapse. J Neurosci. 2003; 23:4092–4099. [PubMed: 12764096]

Parsons TD, Lenzi D, Almers W, Roberts WM. Calcium-triggered exocytosis and endocytosis in an isolated pre-synaptic cell: capacitance measurements in saccular hair cells. Neuron. 1994; 13:875–883. [PubMed: 7946334]

Pfeiffer RR, Kiang NY. Spike discharge patterns of spontaneous and continuously stimulated activity in the cochlear nucleus of anesthetized cats. Biophys J. 1965; 5:301–316. [PubMed: 19431335]

Polishchuk EV, Di Pentima A, Luini A, Polishchuk RS. Mechanism of constitutive export from the golgi: bulk flow via the formation, protrusion, and en bloc cleavage of large trans-golgi network tubular domains. Mol Biol Cell. 2003; 14:4470–4485. [PubMed: 12937271]

Roberts WM, Jacobs RA, Hudspeth AJ. Colocalization of ion channels involved in frequency selectivity and synaptic transmission at presynaptic active zones of hair cells. J Neurosci. 1990; 10:3664–3684. [PubMed: 1700083]

Schmitz F. The making of synaptic ribbons: how they are built and what they do. Neuroscientist. 2009; 15:611–624. [PubMed: 19700740]

Schmitz F, Konigstorfer A, Sudhof TC. RIBEYE, a component of synaptic ribbons: a protein's journey through evolution provides insight into synaptic ribbon function. Neuron. 2000; 28:857–872. [PubMed: 11163272]

Schnee ME, Lawton DM, Furness DN, Benke TA, Ricci AJ. Auditory hair cell-afferent fiber synapses are specialized to operate at their best frequencies. Neuron. 2005; 47:243–254. [PubMed: 16039566]

Schwarz K, Natarajan S, Kassas N, Vitale N, Schmitz F. The synaptic ribbon is a site of phosphatidic acid generation in ribbon synapses. J Neurosci. 2011; 31:15996–16011. [PubMed: 22049442]

Snellman J, Mehta B, Babai N, Bartoletti TM, Akmentin W, Francis A, Matthews G, Thoreson W, Zenisek D. Acute destruction of the synaptic ribbon reveals a role for the ribbon in vesicle priming. Nat Neurosci. 2011; 14:1135–1141. [PubMed: 21785435]

Spassova MA, Avissar M, Furman AC, Crumling MA, Saunders JC, Parsons TD. Evidence that rapid vesicle replenishment of the synaptic ribbon mediates recovery from short-term adaptation at the hair cell afferent synapse. J Assoc Res Otolaryngol. 2004; 5:376–390. [PubMed: 15675002]

Sterling P, Matthews G. Structure and function of ribbon synapses. Trends Neurosci. 2005; 28:20–29. [PubMed: 15626493]

Taberner AM, Liberman MC. Response properties of single auditory nerve fibers in the mouse. J Neurophysiol. 2005; 93:557–569. [PubMed: 15456804]

von Gersdorff H, Vardi E, Matthews G, Sterling P. Evidence that vesicles on the synaptic ribbon of retinal bipolar neurons can be rapidly released. Neuron. 1996; 16:1221–1227. [PubMed: 8663998]

Weigert R, Silletta MG, Spano S, Turacchio G, Cericola C, Colanzi A, Senatore S, Mancini R, Polishchuk EV, Salmona M, Facchiano F, Burger KN, Mironov A, Luini A, Corda D. CtBP/BARS induces fission of Golgi membranes by acylating lysophosphatidic acid. Nature. 1999; 402:429–433. [PubMed: 10586885]

Yang JS, Lee SY, Spano S, Gad H, Zhang L, Nie Z, Bonazzi M, Corda D, Luini A, Hsu VW. A role for BARS at the fission step of COPI vesicle formation from Golgi membrane. EMBO J. 2005; 24:4133–4143. [PubMed: 16292346]

Zampighi GA, Schietroma C, Zampighi LM, Woodruff M, Wright EM, Brecha NC. Conical tomography of a ribbon synapse: structural evidence for vesicle fusion. PLoS One. 2011; 6:e16944. [PubMed: 21390245]

Zenisek D. Vesicle association and exocytosis at ribbon and extraribbon sites in retinal bipolar cell presynaptic terminals. Proc Natl Acad Sci U S A. 2008; 105:4922–4927. [PubMed: 18339810]

Zenisek D, Davila V, Wan L, Almers W. Imaging calcium entry sites and ribbon structures in two presynaptic cells. J Neurosci. 2003; 23:2538–2548. [PubMed: 12684438]

Zenisek D, Horst NK, Merrifield C, Sterling P, Matthews G. Visualizing synaptic ribbons in the living cell. J Neurosci. 2004; 24:9752–9759. [PubMed: 15525760]

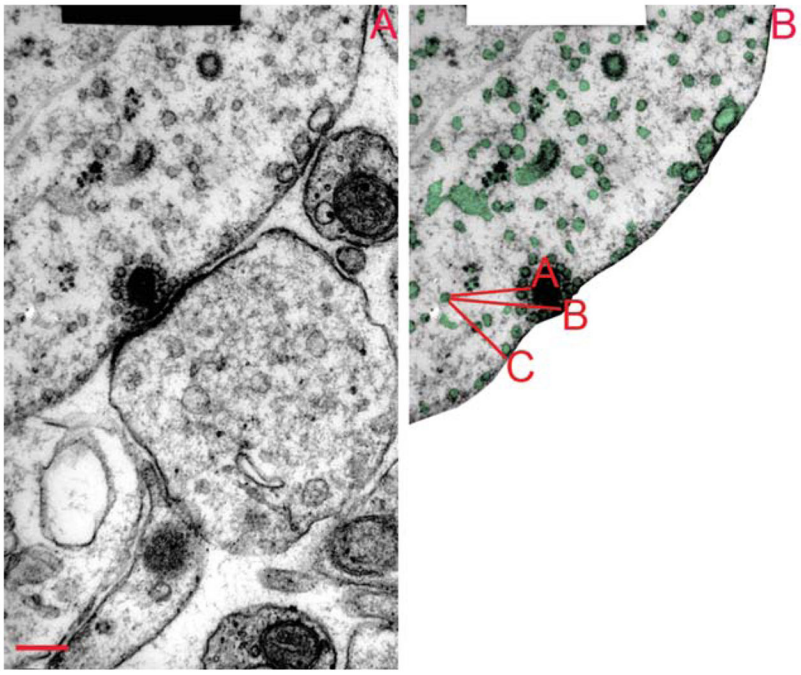

Figure 1.

Analysis of membranous structures near the ribbon synapse. **A:** The micrograph shows a section through a low-SR synapse, approximately in the middle of the ribbon. **B:** Each membrane-enclosed structure in the hair cell was given a number (not included in the picture), then it was outlined, and the distance between the structure and three points of reference (**A:** surface of the ribbon, B; base of the ribbon and **C:** presynaptic membrane) were measured. From the outline, size and degree of circularity were computed. SR =spontaneous rate. Scale bar =200 nm in A (applies to A, B).

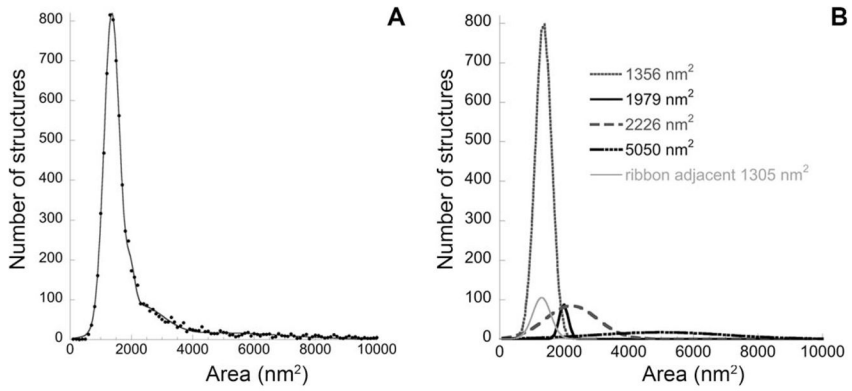

Figure 2.

Size distribution of membranous structures near the synapse (A) can be decomposed into four Gaussian distributions (B). **A:** The distribution of cross-sectional areas of all membranous structures within 2 μm of the synaptic ribbon, from all reconstructed synapses in the study (black circles) is well fit as the sum of four Gaussian distributions (gray line). Although areas as large as 57,000 nm^2 were observed (rarely), the abscissa is truncated at 10,000 nm^2. **B:** All of the four fitted Gaussian distributions, as well as the subset of ribbon adjacent vesicles, are plotted and referenced by the median area. Note that the Gaussian distribution at 1,356 nm^2 includes the separately plotted ribbon adjacent vesicles.

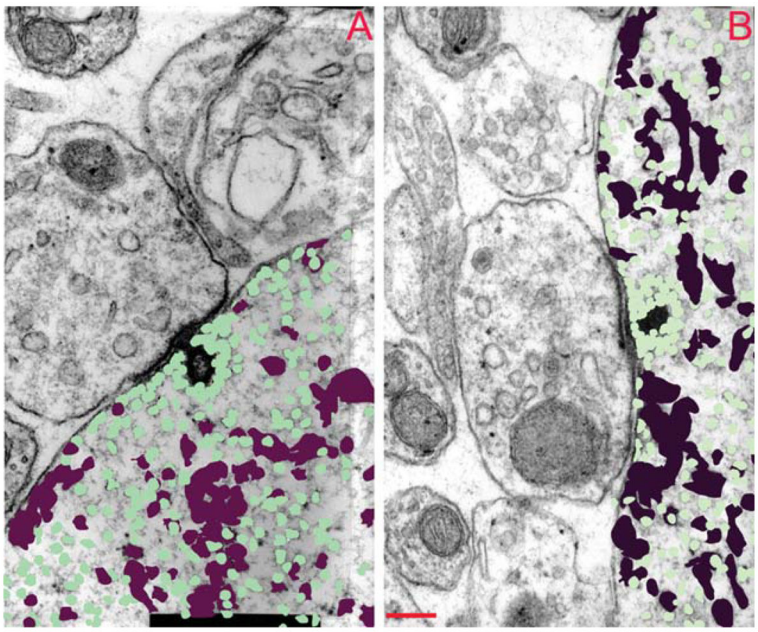

Figure 3.

Spatial distribution of vesicles and cisterns around the ribbon. Sections through a high-SR (**A**) and a low-SR (**B**) synapse containing the synaptic ribbon are shown with the cisternal (maroon) and vesicular (green) profiles colorized. Three profiles are superimposed: the section illustrated as well as the prior and subsequent sections in the series. SR, spontaneous rate. Scale bar= 200 nm in B (applies to A, B)

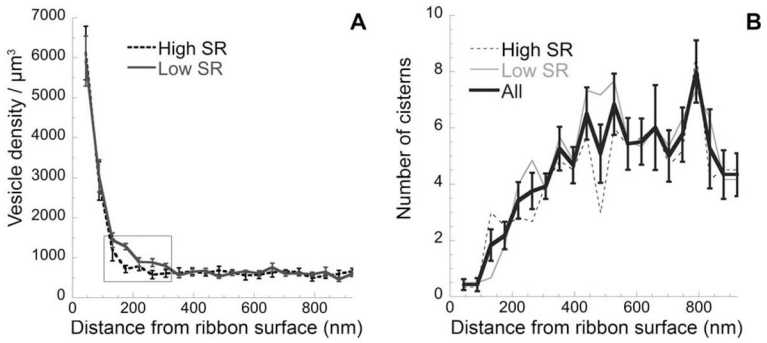

Figure 4.

Distribution of cisterns and vesicles as a function of distance from the ribbon surface. **A:** Mean vesicle density (± SE) for six high-SR and six low-SR synapses. To calculate density (/µm^3), the area of each concentric ring around the ribbon (incremented in 44-µm steps) was multiplied by the section thickness (70 nm). For both panels, only sections including a portion of the ribbon were included. Rectangle indicates the area of significant differences between low- and high-SR synapses. **B:** Mean cisternal counts (± SE) for all synapses are shown. In addition, counts for low- and high-SR synapses are plotted separately. SE, standard error; SR, spontaneous rate.

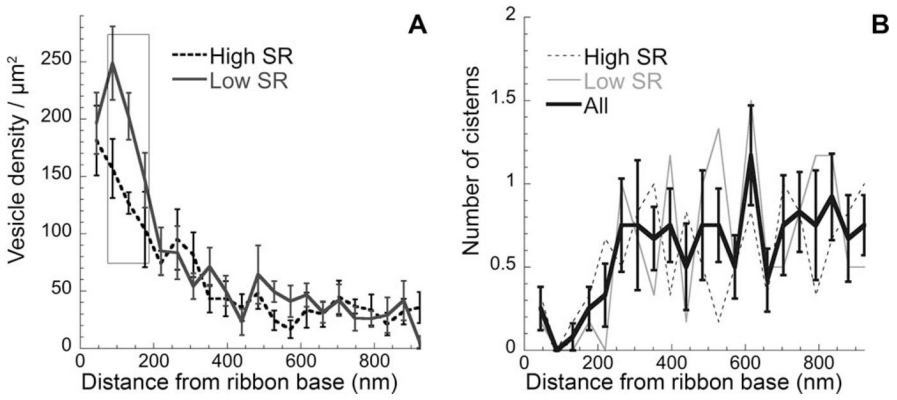

Figure 5.

Distribution of docked vesicles and cisterns. **A:** Mean density (± SE) of docked vesicles, i.e., within 20 nm of the presynaptic density along the presynaptic membrane. **B:** Mean number (± SE) of cisterns within 20 nm of the presynaptic density versus distance along the presynaptic membrane is shown for all synapses. In addition, counts for low- and high-SR synapses are plotted separately. Rectangle indicates the area of significant differences between low- and high-SR synapses. SE, standard error; SR, spontaneous rate.

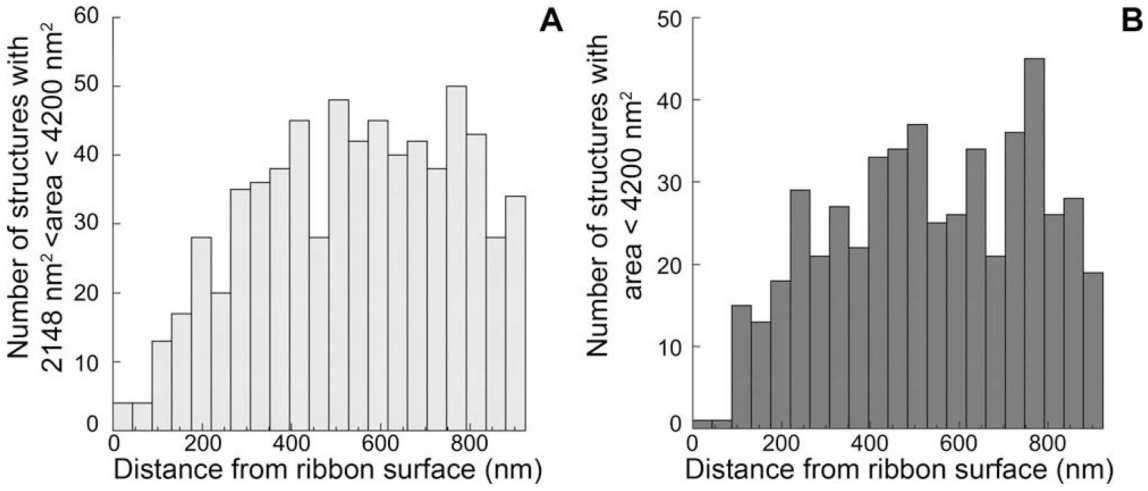

Figure 6.

Spatial distribution of intermediate-sized membranous structures. **A, B:** Gaussian fits to the distribution of membranous structures indicated an intermediate population (dashed gray line in Fig. 2B) with a median size (2,226 nm^2), larger than vesicles but significantly overlapping. Most structures with areas between 2,148 and 4,200 nm^2 (A) were members of that population. With respect to spatial distribution, this population (A) behaved more like cisterns (B) than vesicles, i.e., showed higher density farther from the ribbon surface.

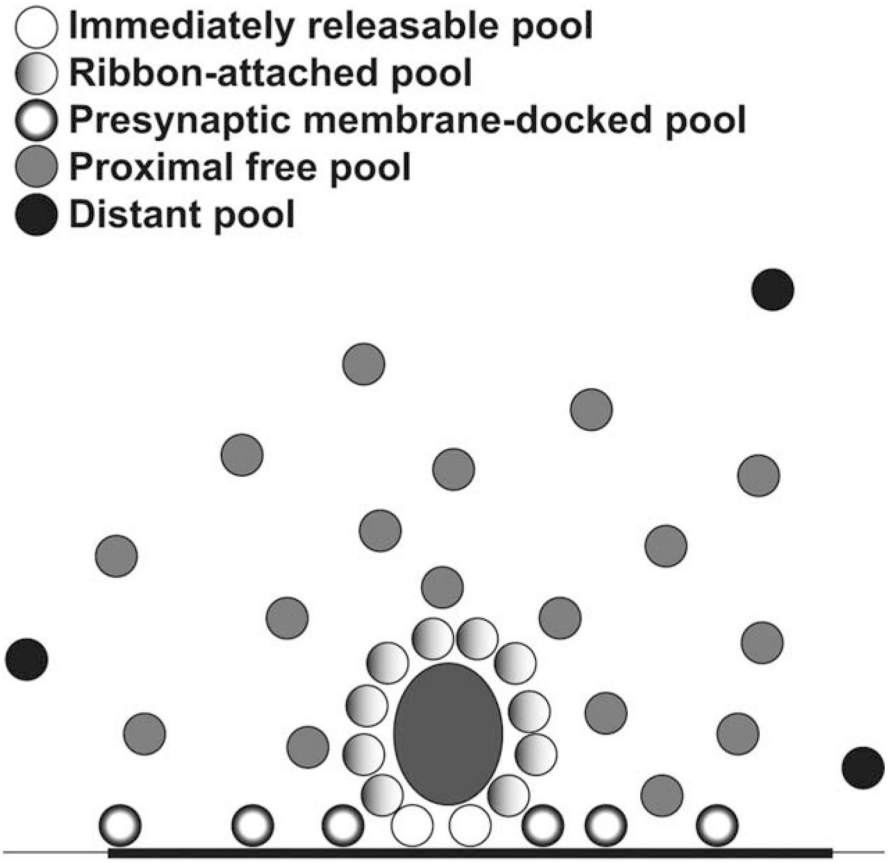

Figure 7.

Schematic showing the observed proportions of vesicles in the different pools. Numbers of vesicle shown reflect the proportions quantified in our analysis. See the key on the figure for: the immediately releasable pool, located beneath the ribbon at the active zone; ribbon-attached vesicles, within 30 nm of the ribbon surface in the side-gradient; presynaptic membrane-docked vesicles located on the active zone; the proximal free pool of vesicles not docked on the ribbon, but located within its sphere of influence 350 nm; and the distant pool located outside the ribbon's sphere of influence. The active zone is indicated by the thickened stroke of the black line representing the presynaptic membrane.

TABLE 1

Comparison of Measurements for High-SR versus low-SR synapses[1]

Feature	High-SR synapse	Low-SR synapse	High/Low ratio
Synaptic ribbon			
Length (nm)	245 (30)	338(38)	0.72
Width (nm)	86.1 (4.4)	84.8 (5.1)	1.02
Height (nm)	150.7 (13.6)	135.4 (3.7)	1.11
Volume (nm^3)	3,139,274 (96,681)	3,267,930 (196,015)	0.96
Surface area (nm^2)	119,198 (5,377)	138,034 (12,444)	0.86
Synaptic densities			
Active zone area (nm^2)	310,371 (24,735)	377,186 (63,181)	0.82
Active zone length (nm/section)	752 (22)	705 (22)	
Presynaptic density length (nm/section)	799 (37)	741 (29)	
Postsynaptic density length (nm/section)	794 (39)	724 (32)	
Presynaptic area beneath ribbon (nm^2)	56,350 (5,499)	77,817 (8,736)	0.72
Vesicles on ribbon surface			
No. excluding immediately releasable pool	34.7 (3.3)	39.3 (6.6)	0.88
No. including immediately releasable pool	42.8 (3.3)	51.3 (8.3)	0.83
Density including immediately releasable pool (/μm^2)	362.9 (30.6)	360.8 (33.7)	1
Vesicles docked on the presynaptic density			
No.	44.2 (6.1)	56.9 (10.1)	0.77
Density (/μm^2)	145.2 (20.9)	157.6 (18.2)	0.92
Vesicles beneath ribbon (immediately releasable pool)			
No.	8.2 (1.1)	12 (1.8)	0.68
Density (/μm^2)	149.8 (25.4)	153 (14.8)	0.98
Vesicles in the proximal free pool* (P =0.015)	78.5 (7.8)	109.7 (7.4)	0.72
Vesicles (% total area)	7.34 (0.66)	7.90 (0.20)	0.93
Cisterns (% total area)	8.36 (1.00)	10.71 (1.15)	0.78
Average mitochondrial content of afferent fibers* (P =0.001)	1.68 (0.07)	0.69 (0.04)	2.42

[1] Standard error (SE) is in parentheses. SR, spontaneous rate.

* Significant differences between low- and high-SR synapses.